# Kondo memory in driven strongly-correlated quantum dots

Xiao Zheng,[1, *] YiJing Yan,[1, 2] and Massimiliano Di Ventra[3, †]

[1]Hefei National Laboratory for Physical Sciences at the Microscale,
University of Science and Technology of China, Hefei, Anhui 230026, China
[2]Department of Chemistry, Hong Kong University of Science and Technology, Kowloon, Hong Kong, China
[3]Department of Physics, University of California, San Diego, La Jolla, California 92093
(Dated: April 9, 2013)

We investigate the real-time current response of strongly-correlated quantum dot systems under sinusoidal driving voltages. By means of an accurate hierarchical equations of motion approach, we demonstrate the presence of prominent memory effects induced by the Kondo resonance on the real-time current response. These memory effects appear as distinctive hysteresis line shapes and self-crossing features in the dynamic current-voltage characteristics, with concomitant excitation of odd-number overtones. They emerge as a cooperative effect of quantum coherence – due to inductive behavior – and electron correlations – due to the Kondo resonance. We also show the suppression of memory effects and the transition to classical behavior as a function of temperature. All these phenomena can be observed in experiments and may lead to novel quantum memory applications.

Memory of physical systems is quite a common phenomenon [1]. It simply means that the state of a system at a given time – driven by an external input – depends strongly on its history, at least within a certain range of parameters of the external drive, such as its frequency or amplitude [1, 2]. These memory features give rise to unconventional properties and novel functionalities that can be used in actual device applications.

Although there has been a recent crescendo of interest in memory effects in resistive, capacitive and inductive systems [3], less work has been devoted to memory effects in strongly-correlated quantum systems. These include the single-molecule magnets [4, 5], metal-oxide-semiconductor thin films [6, 7], nanoparticle assemblies [8], and bulk Kondo insulators [9]. In this respect, quantum dots (QDs) coupled to electron reservoirs are ideal platforms for experimental and theoretical studies relevant to quantum computation and quantum information [10, 11]. This is because the electron or spin state of a QD can be manipulated conveniently by external fields, with the quantum coherence largely preserved. In particular, at low temperatures, formation of the Kondo singlet state [12–15] opens up additional channels for electron conduction. However, it is not at all obvious if new features would emerge due to the interplay between quantum coherence and electron correlations under driving conditions, and if the Kondo phenomena would influence significantly the memory of the QD system.

In this letter we show that Kondo resonances indeed induce prominent memory effects when a QD is driven by an external periodic voltage. These features appear as well-defined hysteresis line shapes and self-crossing features in the dynamic current-voltage characteristics with excitation of odd-number overtones. They are a direct consequence of quantum coherence and electron correlations and are suppressed at relatively high temperatures

where a classical behavior is recovered. All these effects can be probed at specific frequencies that are within reach of experimental verification.

The QD system of interest is illustrated with a single-impurity Anderson model [16], $H_{\rm dot} = \epsilon_d(\hat{n}_\uparrow + \hat{n}_\downarrow) + U\hat{n}_\uparrow\hat{n}_\downarrow$. Here, $\hat{n}_s = \hat{a}_s^\dagger \hat{a}_s$, and $\hat{a}_s^\dagger$ $(\hat{a}_s)$ creates (annihilates) a spin-$s$ electron on the dot level of energy $\epsilon_d$, while $U$ is the on-dot electron-electron ($e$-$e$) interaction strength. The total Hamiltonian is

$$H = H_{\rm dot} + H_{\rm res} + H_{\rm coupling}, \qquad (1)$$

with $H_{\rm res} = \sum_{\alpha k} \epsilon_{\alpha k} d_{\alpha k}^\dagger d_{\alpha k}$ and $H_{\rm coupling} = \sum_{\alpha k} t_{\alpha k} a_s^\dagger d_{\alpha k} + {\rm H.c.}$, for the noninteracting leads and the dot-lead couplings, respectively. Here, $d_{\alpha k}^\dagger$ $(d_{\alpha k})$ is the creation (annihilation) operator for the $\alpha$-lead state $|k\rangle$ of energy $\epsilon_{\alpha k}$, and $t_{\alpha k}$ is the coupling strength between the dot level and $|k\rangle$. For numerical convenience, identical leads are considered, and their hybridization functions assume a Lorentzian form, $\Delta_\alpha(\omega) \equiv \pi \sum_k t_{\alpha k} t_{\alpha k}^* \delta(\omega - \epsilon_{\alpha k}) = \Delta W^2/2[(\omega - \mu_\alpha)^2 + W^2]$, where $\Delta$ is the effective dot-lead coupling strength, $W$ is the band width, and $\mu_\alpha$ is the chemical potential of the $\alpha$-lead. We prepare the initial total system at equilibrium, where $\mu_\alpha = \mu^{\rm eq} \equiv 0$. An $ac$ voltage is applied to the left (L) and right (R) leads from the time $t_0 \equiv 0$, i.e., $V_{\rm L}(t) = -V_{\rm R}(t) = V_0 \sin(\Omega t)$, with $V_0$ and $\Omega$ being the voltage amplitude and frequency, respectively. Upon switching on the voltage, the QD is driven out of equilibrium, and the time-dependent current flowing into the $\alpha$-lead $\bar{I}_\alpha(t)$ is computed.

To proceed, a choice of method for calculating current must be made that accurately reproduces the nonequilibrium electronic dynamics of this strongly correlated electron system. A number of theoretical approaches have been developed to tackle this problem, such as the time-dependent numerical renormalization group (NRG) approach [17], the time-dependent density matrix renormal-

ization group approach [18, 19], the real-time diagrammatic quantum Monte Carlo [20, 21], the Kadanoff–Baym time-dependent Green's function approach [22, 23], the time-dependent density-functional theory [24], and quantum master equation approaches [5, 25–27]. For instance, the time scale for the buildup of Kondo resonance in a strongly correlated QD has been studied by using a Green's function technique, where the $e$-$e$ interaction is accounted for within the noncrossing approximation [28, 29].

We choose the hierarchical equations of motion (HEOM) approach, developed in recent years by Yan and coworkers [30–32]. This is a unified, real-time approach for a wide range of equilibrium and nonequilibrium, static and dynamic properties of a general open quantum system [32–35]. The basic variables in HEOM are the reduced density matrix of the open system and a set of auxiliary density matrices. The HEOM approach has been employed to study, for instance, the dynamic Coulomb blockade and dynamic Kondo phenomena in QDs [36, 37]. To close the coupled equations, the hierarchy needs to be truncated at a certain level $L$. In principle, the exact solution is guaranteed for $L \rightarrow \infty$. In practice, the results usually converge rapidly with increasing $L$ at finite temperatures. Once the convergence is achieved, the numerical outcome is considered to be quantitatively accurate. For instance, it has been demonstrated that the HEOM approach achieves the same level of accuracy as the latest NRG method for the prediction of various dynamical properties at equilibrium [32], and it has reproduced [33] the exact numerical solution for the time-dependent current response of a noninteracting QD to a step-function bias voltage [38, 39]. Here, we solve the HEOM dynamics described by Hamiltonian (1), at the $L = 4$ truncation level of hierarchy [36, 37] (see also Supplemental Material [40]). We have checked that all results presented in this letter converge quantitatively with respect to this truncation.

Figure 1 depicts the dynamic $I$-$V$ characteristics of a QD which possesses the electron-hole symmetry ($U = -2\epsilon_d$) subject to an $ac$ voltage of various frequencies $\Omega$. To compare with the energetic parameters of the QD, $\Omega$ is represented by the harmonic energy associated with the driving voltage. In particular, $\Omega = 0.01$ meV corresponds to a period of $0.4$ ns. Although high, these GHz time-domain voltage manipulations and current measurements have been realized experimentally [41–43]. The calculation results indicate that the electron-hole symmetry is preserved under the $ac$ voltage, and the dot level is always half-filled. Consequently, the displacement current is zero, and the Kirchhoff's current law holds at any time, i.e., $I(t) = \bar{I}_{\mathrm{R}}(t) = -\bar{I}_{\mathrm{L}}(t)$ [5].

As shown in Fig. 1(a), at a low $\Omega$, the dynamic $I$-$V$ characteristics is close to the steady-state curve, since the electrons have sufficient time to redistribute to catch up with the variation of voltage. In contrast, at a high
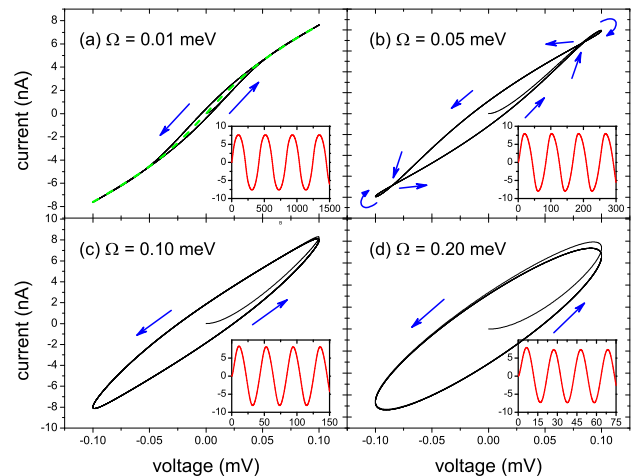


FIG. 1: (Color online). Current versus voltage for a QD driven by an $ac$ voltage of amplitude $V_0 = 0.1$ mV and frequency $\Omega$. The arrows indicate the circulating directions of the loops. The green dashed curve in (a) depicts the steady-state $I$-$V$ characteristics. The insets plot the corresponding current (in nA) versus time (in ps). The other parameters (in meV) are $U = -2\epsilon_d = 0.4$, $\Delta = 0.1$, $W = 2$, and $T = 0.02$.

$\Omega$, the dynamic $I$-$V$ curve forms an ellipse; see Fig. 1(d). The ellipse shape originates from a phase difference between the current and voltage. In the case of Fig. 1(d), the ellipse is traversed in the counterclockwise direction (voltage leads current), indicating a prominent inductive behavior. It has been demonstrated that in the linear response regime a two-terminal device can be mapped onto a classical circuit, where a resistor-capacitor branch and a resistor-inductor branch are connected in parallel [44–46]. Here, the inductance is associated with the time for an electron to dwell on the device [44, 47] and is due to the fact that the dot energy is lower than the equilibrium energy, as required in order to have a Kondo resonance. At an intermediate $\Omega$, the dynamic $I$-$V$ curve forms a hysteresis loop with self-crossing in the first and third quadrants; see Fig. 1(b). The hysteresis behavior highlights the nontrivial memory effects on the real-time electron dynamics. To understand further these memory effects, we vary both the coupling strength $U$ and the temperature $T$.

Figure 2 plots the dynamic $I$-$V$ curves for a series of symmetric QDs of different $U$ under the same driving voltage and temperature $T$. The hysteresis behavior of Fig. 1(b) is constantly observed. It is interesting to see that the $I$-$V$ curve shape varies in a non-monotonic manner with respect to $U$, and the hysteresis behavior is most outstanding at around $U = 1.2$ meV. To understand this trend, we calculate the steady-state differential conductances ($dI/dV$) of the QD under the bias voltage $V_{\mathrm{L}} = -V_{\mathrm{R}} = V$. The resulting $dI/dV$ are then scaled by their respective values at $V = 0$. These curves are shown in Fig. 2(d). The differential
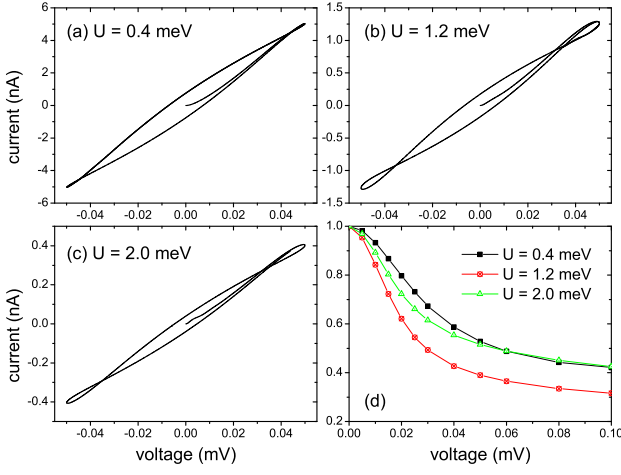
FIG. 2: (Color online). Current versus voltage for the QDs of (a) $U = 0.4$, (b) $U = 1.2$, and (c) $U = 2$ meV, under the antisymmetric $ac$ voltage of $V_0 = 0.05$ mV and $\Omega = 0.03$ meV. Panel (d) shows the steady-state $dI/dV$ versus the bias voltage $V = V_L = -V_R$, where the displayed data are scaled by the value of $dI/dV$ at $V = 0$. The other parameters (in meV) are $\epsilon_d = -U/2$, $\Delta = 0.1$, $W = 2$, and $T = 0.01$.

conductance clearly decays nonlinearly with increasing voltage, and $U = 1.2$ meV corresponds to the steepest descent of $dI/dV$. The maximal conductance at $V = 0$ is due to the formation of Kondo states. Under a bias voltage, the Kondo channel is blocked by the gap between the chemical potentials in the two leads, leading to the drastic decay in conductance with increasing $V$. This is confirmed by the evolution of the Kondo spectral signature versus voltage (see Supplemental Material [40]). For the QD studied in Fig. 2, the Kondo temperatures $T_K = (U\Delta/2)^{1/2} \exp[-\pi U/8\Delta + \pi\Delta/2U]$ are $0.044$, $2.5 \times 10^{-3}$ and $1.3 \times 10^{-4}$ meV for $U = 0.4$, $1.2$ and $2$ meV, respectively. Therefore, under a fixed temperature, the Kondo resonance would lead to a steeper decay in $dI/dV$ with a smaller $U$. On the other hand, the dot level of energy $\epsilon_d = -U/2$ becomes closer to $\mu^{eq}$ as $U$ diminishes. This provides another conduction channel with width $\Delta$, and its associated conductance decays much more slowly than the Kondo channel since $T_K \ll \Delta$. With the presence of both conduction channels, the steepest decay in $dI/dV$ occurs at an intermediate value of $U$.

The shape of the dynamic $I$-$V$ characteristics can now be interpreted as follows. In the limit of adiabatic driving ($\Omega \to 0$), the evolution of the current response follows exactly the steady-state $dI/dV$-$V$ curve. The reduction in $dI/dV$ versus $V$ leads to a concave $I$-$V$ curve at $V > 0$; see the green dotted line in Fig. 1(a). At a finite $\Omega$, the inductive feature starts to emerge, which forces the current to lag behind the driving voltage. For instance, at an instant when the voltage turns from negative to positive, the current has not yet reached its turning point

– it remains negative but accelerates toward the voltage. Consequently, the dynamic $I$-$V$ curve has a convex curvature at $V = 0$ and $I < 0$. The convexity may be inverted into concavity provided that the increase in voltage captures the drastic decay in conductance. This requires a relatively low $\Omega$, with which the variation of "transient" conductance does not deviate much from the steady-state $dI/dV$-$V$ curve shown in Fig. 2(d). Such a convex-concave curve segment, together with its mirror-image counterpart upon voltage decrease, results in a self-crossing hysteresis loop as depicted in Fig. 1(b) and Fig. 2(a)-(c). At a high $\Omega$, there is not enough time for the buildup of Kondo states, and thus the $dI/dV$-$V$ curve is effectively smoothed. In this case, the inductive feature becomes a dominant factor, and the dynamic $I$-$V$ curve displays a simple ellipse shape; see Fig. 1(d).

Based on the above analysis, we can conclude that the hysteresis behavior of the $ac$ $I$-$V$ characteristics originates from a cooperative interplay between the quantum coherence (the inductive feature) and strong electron correlation (the Kondo resonance). Since both quantum coherence and correlation are significantly influenced by thermal fluctuations, the associated memory effects are expected to depend sensitively on the temperature.

In Fig. 3(a) we show the evolution of the dynamic $I$-$V$ curve with increasing temperature. Here, in order to accentuate the nonlinear current response, a somewhat larger voltage amplitude ($V_0 = 0.1$ meV) is adopted. At low temperature ($T = 0.01$ meV), the $ac$ $I$-$V$ curve displays a remarkable hysteresis behavior, with the emergence of multiple self-crossing points. Such a convoluted line shape is a strong indication of complex memory effects. With the temperature rising by as little as $0.01$ meV, the hysteresis behavior of Fig. 2(b) is recovered, with only one crossing in the first or third quadrant. This apparent change in the hysteresis pattern should be ascribed to the suppression of the Kondo resonance. Indeed, as shown clearly in Fig. 3(c), the zero-bias conductance decays drastically with a minor increase in $T$ from $0.01$ meV. Meanwhile, increasing $T$ leads to the progressive narrowing of the $I$-$V$ hysteresis loop, and the loop almost merges into a single line at $T = 0.1$ meV. This means that the inductive feature becomes irrelevant at a high temperature, and the QD behaves like a classical resistor. This is because the conducting electrons have a wide energy distribution due to thermal excitations, and the phase difference between the current and voltage is largely randomized. Due to the same reason, the steady-state $dI/dV$ varies rather smoothly as a function of $V$ at high $T$, leading to an overall Ohmic conductance.

The temperature-sensitive memory is further explored through a frequency analysis of the response current. The current spectrum for a single-lead QD under sinusoidal voltages has been studied in Ref. 45, where the response current signals concentrate on the exact multiples of driving frequency $\Omega$. For the two-terminal QD investigated
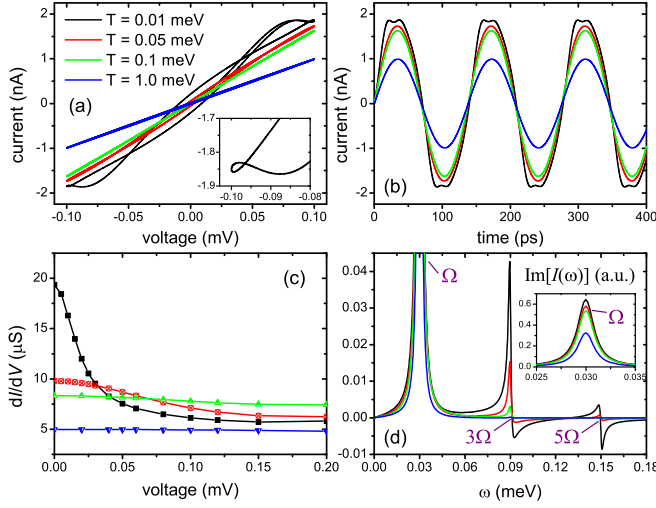
FIG. 3: (Color online). (a) Dynamic $I$-$V$ characteristics, (b) real-time current response, (c) steady-state $dI/dV$ versus $V$, and (d) imaginary part of current spectrum of a QD with $U = -2\epsilon_d = 1.2\,\text{meV}$ at various temperatures. The inset of (a) magnifies the self-crossing of $ac$ $I$-$V$ curve near $V = -V_0$ at $T = 0.01\,\text{meV}$, and that of (b) displays the full peaks of $\text{Im}[I(\omega)]$ at $\omega = \Omega$. The other parameters (in meV) are $\Delta = 0.1$, $W = 2$, $V_0 = 0.1$, and $\Omega = 0.03$.

here, the variation of current spectrum versus temperature is depicted in Fig. 3(d). It is found that the response current arises predominantly at $\omega = (2n + 1)\Omega$ with $n \in \mathbb{Z}$, while the even overtones remain unexcited. This is because the $ac$ voltages have the left-right anti-symmetry, so that the response current would flow in the reverse direction if the half-period were taken as the initial time ($t_0 = \pi/\Omega$). Therefore, the relation $I(\omega) = -I(\omega)e^{i\omega\pi/\Omega}$ must be satisfied. Overtones of all symmetries can be found by breaking the symmetric coupling between the QD and the leads [48]. As $T$ rises from 0.01 to 0.1 meV, the change in current amplitude at the fundamental frequency is rather minor. In contrast, the overtone responses vanish almost completely. This highlights the dynamic Kondo-assisted electron conduction, which requires a relatively low excitation energy. At $T < 0.01\,\text{meV}$, the Kondo memory effects are expected to be even more prominent. However, to achieve convergent HEOM results at a lower $T$, a higher truncation level $L$ is required, which is numerically too demanding with the present computational resources at our disposal. At $T > 0.1\,\text{meV}$, the Kondo resonance is absent, and the dot level is away from the resonance region ($|\epsilon_d| > V_0$). Consequently, the system falls in the linear response regime, and the corresponding real-time current becomes synchronized with the voltage; see Fig. 3(b).

We finally present some considerations on the experimental verification of our predictions. In realistic experimental setups, a QD may involve more than one energy level and more complicated forms of $e$-$e$ interaction.
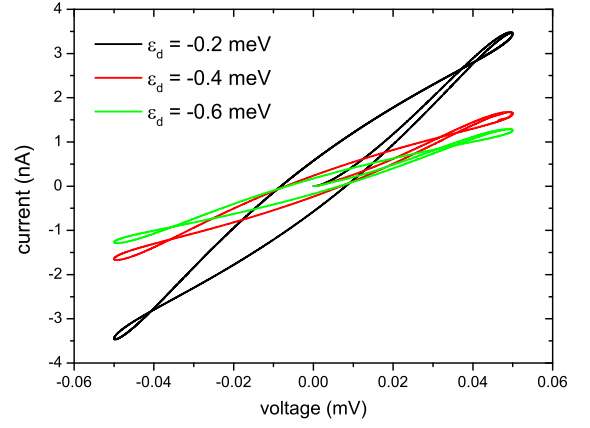


FIG. 4: (Color online). Dynamic $I$-$V$ characteristics of QDs with different $\epsilon_d$. The displayed current is $I(t) = [\bar{I}_R(t) - \bar{I}_L(t)]/2$. The other parameters (in meV) are $\Delta = 0.1$, $U = 1.2$, $T = 0.01$, $W = 2$, $V_0 = 0.05$, and $\Omega = 0.03$.

Therefore, the memory effects will influence the real-time dynamics in a rather complex way. However, since the Kondo resonance is tightly tied to the lead chemical potential, the Kondo memory may be identified distinctly from other memory effects. For instance, consider the scenario where the dot-level $\epsilon_d$ is shifted by a gate voltage, and the $ac$ $I$-$V$ curves at different $\epsilon_d$ are shown in Fig. 4. At $U \neq -2\epsilon_d$, the electron-hole symmetry is broken, and transient charging takes place at the QD. To concentrate on the net conduction current, the displacement component is taken care of by symmetrizing the left- and right-lead currents [5]. As clearly indicated in Fig. 4, the Kondo-resonance-induced hysteresis behavior is continually preserved with $\epsilon_d$ shifted by as much as 0.4 meV. Since any single-electron resonance associated with a dot energy level would have been switched off under such a large gate voltage, Fig. 4 accentuates the robustness of Kondo memory effects.

To conclude, we have demonstrated the presence of Kondo-resonance-induced memory effects in the real-time electronic dynamics of strongly correlated QDs, which may be observed in experiments. The predicted hysteresis line shape and self-crossing features of the $ac$ $I$-$V$ characteristics highlight the remarkable interplay between quantum coherence and quantum electron correlations. These effects may lead to novel applications of QDs in the Kondo regime, ranging from machine learning [49] to massively-parallel computation and information processing [50].

the Center for Magnetic Recording Research at UCSD.

* Electronic address: xz58@ustc.edu.cn
† Electronic address: diventra@physics.ucsd.edu
[1] Y. V. Pershin and M. Di Ventra, Adv. Phys. **60**, 145 (2011).
[2] J. J. Yang, D. B. Strukov, and D. R. Stewart, Nature Nanotech. **8**, 13 (2013).
[3] M. Di Ventra, Y. V. Pershin, and L. O. Chua, Proceedings of the IEEE **97**, 1717 (2009).
[4] T. Miyamachi et al., Nature Comm. **3**, 938 (2012).
[5] C. Timm and M. Di Ventra, Phys. Rev. B **86**, 104427 (2012).
[6] D. B. Strukov, G. S. Snider, D. R. Stewart, and R. S. Williams, Nature **453**, 80 (2008).
[7] Z.-J. Liu, J.-Y. Gan, and T.-R. Yew, Appl. Phys. Lett. **100**, 153503 (2012).
[8] T. H. Kim et al., Nano Lett. **9**, 2229 (2009).
[9] D. J. Kim and Z. Fisk, Appl. Phys. Lett. **101**, 013505 (2012).
[10] D. Loss and D. P. DiVincenzo, Phys. Rev. A **57**, 120 (1998).
[11] A. Imamoğlu et al., Phys. Rev. Lett. **83**, 4204 (1999).
[12] L. I. Glazman and M. E. Raikh, JETP Lett. **47**, 452 (1988).
[13] T. K. Ng and P. A. Lee, Phys. Rev. Lett. **61**, 1768 (1988).
[14] Y. Meir, N. S. Wingreen, and P. A. Lee, Phys. Rev. Lett. **70**, 2601 (1993).
[15] D. Goldhaber-Gordon et al., Nature **391**, 156 (1998).
[16] P. W. Anderson, Phys. Rev. **124**, 41 (1961).
[17] F. B. Anders and A. Schiller, Phys. Rev. Lett. **95**, 196801 (2005).
[18] M. A. Cazalilla and J. B. Marston, Phys. Rev. Lett. **88**, 256403 (2002).
[19] S. R. White and A. E. Feiguin, Phys. Rev. Lett. **93**, 076401 (2004).
[20] P. Werner, T. Oka, and A. J. Millis, Phys. Rev. B **79**, 035320 (2009).
[21] M. Schiró and M. Fabrizio, Phys. Rev. B **79**, 153302 (2009).
[22] P. Myöhänen, A. Stan, G. Stefanucci, and R. van Leeuwen, Europhys. Lett. **84**, 67001 (2008).
[23] K. S. Thygesen and A. Rubio, Phys. Rev. B **77**, 115333 (2008).
[24] S. Kurth, G. Stefanucci, E. Khosravi, C. Verdozzi, and E. K. U. Gross, Phys. Rev. Lett. **104**, 236801 (2010).
[25] P. Cui, X. Q. Li, J. S. Shao, and Y. J. Yan, Phys. Lett. A **357**, 449 (2006).
[26] X. Q. Li and Y. J. Yan, Phys. Rev. B **75**, 075114 (2007).
[27] J. N. Pedersen and A. Wacker, Phys. Rev. B **72**, 195330 (2005).
[28] P. Nordlander, M. Pustilnik, Y. Meir, N. S. Wingreen, and D. C. Langreth, Phys. Rev. Lett. **83**, 808 (1999).
[29] M. Plihal, D. C. Langreth, and P. Nordlander, Phys. Rev. B **71**, 165321 (2005).
[30] J. S. Jin, X. Zheng, and Y. J. Yan, J. Chem. Phys. **128**, 234703 (2008).
[31] X. Zheng et al., Prog. Chem. **24**, 1129 (2012).
[32] Z. H. Li et al., Phys. Rev. Lett. **109**, 266403 (2012).
[33] X. Zheng, J. S. Jin, and Y. J. Yan, J. Chem. Phys. **129**, 184112 (2008).
[34] X. Zheng, J. Y. Luo, J. S. Jin, and Y. J. Yan, J. Chem. Phys. **130**, 124508 (2009).
[35] S. K. Wang, X. Zheng, J. S. Jin, and Y. J. Yan, arXiv:1301.6850 (2013).
[36] X. Zheng, J. S. Jin, and Y. J. Yan, New J. Phys. **10**, 093016 (2008).
[37] X. Zheng, J. S. Jin, S. Welack, M. Luo, and Y. J. Yan, J. Chem. Phys. **130**, 164708 (2009).
[38] G. Stefanucci and C.-O. Almbladh, Phys. Rev. B **69**, 195318 (2004).
[39] J. Maciejko, J. Wang, and H. Guo, Phys. Rev. B **74**, 085324 (2006).
[40] See the Supplemental Material at xxx for more details on the HEOM formalism and the convergence of numerical results with respect to the truncation level of hierarchy.
[41] J. Gabelli et al., Science **313**, 499 (2006).
[42] G. Fève et al., Science **316**, 1169 (2007).
[43] G. Cao et al., Nat. Commun. **4**, 1401 (2013).
[44] C.-Y. Yam et al., Nanotechnology **19**, 495203 (2008).
[45] Y. Mo, X. Zheng, G. H. Chen, and Y. J. Yan, J. Phys.: Condens. Matter **21**, 355301 (2009).
[46] S. Z. Wen et al., J. Phys. Chem. B **115**, 5519 (2011).
[47] J. Wang, B. Wang, and H. Guo, Phys. Rev. B **75**, 155336 (2007).
[48] G. Z. Cohen, Y. V. Pershin, and M. Di Ventra, Appl. Phys. Lett. **100**, 133109 (2012).
[49] Y. V. Pershin, S. La Fontaine, and M. Di Ventra, Phys. Rev. E **80**, 021926 (2009).
[50] Y. V. Pershin and M. Di Ventra, Phys. Rev. E **84**, 046703 (2011).